PCCP

Accepted Manuscript

ROYAL SOCIETY OF CHEMISTRY

www.rsc.org/pccp

Physical Chemistry Chemical Physics

RSCPublishing

ARTICLE

Controlled growth of extended arrays of CoSi₂ hexagonal nanoplatelets buried in Si(001), Si(011) and Si(111) wafers.

G. Kellermann,[a] L. A. Montoro,[b] L. J. Giovanetti,[c] P. C. dos Santos Claro,[c] L. Zhang ,[d] A. J. Ramirez,[e] F. G. Requejo,[c] and A. F. Craievich,[f]

Because of their high electrical conductivity CoSi₂ nanostructures are potential candidates for preparing ordered nano-arrays to be used as electrodes interconnectors and contacts in microelectronic devices. We here describe a controlled procedure for the endotaxial growth of hexagonal CoSi₂ nanoplatelets buried in differently oriented single crystalline Si wafers on which a Co-doped SiO₂ thin film was previously deposited. These nanomaterials were obtained by a clean procedure consisting of isothermal annealing at 750 °C under He atmosphere of Co-doped SiO₂ thin films deposited onto the surface of three differently oriented flat Si substrates, namely Si(001), Si(011) and Si(111). Buried CoSi₂ nanoplatelets are in all cases spontaneously formed as a consequence of the diffusion of Co atoms into the silicon wafer and their reaction with host Si atoms. Our TEM and GISAXS analyses demonstrated that these arrays, irrespective of host Si orientation, consist of CoSi₂ hexagonal nanoplatelets in all cases parallel to Si{111} crystallographic planes. Additionally, the dimensions of the nanoplatelets were consistently determined by TEM and GISAXS for the three different host Si single crystal orientations.

Introduction

An increasing demand for the development of new methods for preparation of nanomaterials and nanocomposites suited for technological applications has been observed during the last decades.[1–3] The interest for these nanomaterials is related to the fact that many of their properties can be varied in a continuous way by changing the size, shape and/or spatial ordering and integration of their basic nanostructured components.[4,5]

Particularly, silicides of transition metals, as CoSi₂, possess great interest because of the possibilities of applications as contact material for microelectronic devices.[6–11] Thin films of CoSi₂ exhibit a very low electrical resistivity, ρ=10-15 $\mu\Omega$.cm[12], similar to the resistivity of TiSi₂ which is currently used as ohmic contact in microelectronic devices. In order to develop new prototypes, improving their technological perspectives, a challenge is to produce nanomaterials such as nanoparticles, nanorods, nanowires, nanoplatelets, etc with the desired properties and large scale integration. This is expected to be achieved by developing novel procedures to control size, shape, spatial order and integration of the basic nanostructured components[13,14] by controlling the fundamental processes of grow, diffusion, agglomeration, segregation, etc.[13,15–17]

A simple procedure for obtaining buried arrays of CoSi₂ nanoplatelets coherently embedded in a Si(001) host lattice was described in a recently published study[18]. In this investigation it was demonstrated that thermally activated diffusion of Co atoms from supported Co-doped SiO₂ thin film into a flat Si(001) wafer substrate, promotes the formation of a regular array of oriented CoSi₂ nanoplatelets buried in the Si single crystal. The analysis of TEM images indicated that the CoSi₂ nanoplatelets exhibit a CaF₂-like atomic structure, hexagonal lateral shape and a remarkable uniform thickness. The crystal lattice of the CoSi₂ nanoplatelets was demonstrated to be coherent with the host Si lattice and the main surface of the platelets are parallel to Si{111} crystallographic planes.[18]

This work aims at obtaining information about structural features of the CoSi₂ nanostructured array developed in Si substrates with different orientations. For this purpose we have prepared three samples consisting of differently oriented Si substrates, namely Si(001), Si(011) and Si(111), on which SiO₂ thin films were deposited under equivalent preparation conditions. After deposition of the thin film, all studied Si wafers were exposed to the same thermal treatment and then characterized by transmission electron microscopy (TEM) and grazing-incidence small-angle X-ray scattering (GISAXS).

Experimental Section

Sample Preparation:

Silica thin films containing homogeneously dispersed Co atoms deposited on Si(001), Si(111) and Si(011) wafers were obtained by dipping the flat surface of the Si substrates into a solution of cobalt(II) nitrate (11 μmol/g) and tetraethylorthosilicate (TEOS, 240 μmol/g) in isopropanol. After evaporation of the solvent the films were dried during 10 min at 100 C and calcined during 15 min at 500 C. In order to promote the chemical reduction of the precursor molecules thus inducing the formation of Co atoms, the samples (thin film and substrate) were isothermally treated during 1 hour at 500 C under H_2 atmosphere to promote the Co oxide reduction. Finally all samples were subjected to an equivalent isothermal annealing during 1 h at 750 C under He atmosphere. This last thermal process allowed for the diffusion Co atoms thus promoting: (i) the aggregation of Co atoms and further formation of Co nanoparticles (NP) embedded in the SiO_2 thin film and (ii) the formation of $CoSi_2$ nanoplatelets buried in the Si wafer.

Transmission electron microscopy (TEM)

TEM experiments were performed at the Brazilian Nanotechnology National Laboratory (LNNano), Campinas, using a JEM-2100F URP TEM at 200 kV in transmission (TEM) and scanning transmission (STEM) modes. The images were recorded by using CCD cameras and a bright-field (BF) detector. X-ray energy dispersive spectroscopy (XEDS) measurements were performed by using a Si-Li detector coupled to the TEM.

Grazing Incidence Small X-ray Scattering (GISAXS)

GISAXS experiments were conducted at the XRD2 X-ray diffraction beam line of the Brazilian Synchrotron Light Laboratory (LNLS), Campinas, Brazil, using an X-ray beam with a wavelength λ = 0.1612 nm. The scattered photons were recorded using a Pilatus 2D position sensitive detector. A schematic representation of the GISAXS setup is shown in Figure S4 of SI. The selected grazing incidence angle, $\alpha_i = 0.3^o$, slightly above the critical angle for total reflection of SiO_2, corresponds to a penetration depth that maximize the X-ray scattering intensity produced by the $CoSi_2$ nanoplatelets. The footprint of the X-ray beam on the sample surface was (4 x 15) mm^2.

Results and Discussion:

Silica thin films containing homogeneously dispersed Co nanoparticles (NP) deposited on Si(001), Si(111) and Si(011) wafers were obtained by dipping the flat surface of the Si substrates into a solution containing tetraethylorthosilicate and cobalt nitrate as precursors of porous silicon film and metallic cobalt NP respectively. All samples were subjected to an equivalent isothermal annealing during 1 h at 750 C under He atmosphere. This isothermal process promotes the formation of $CoSi_2$ nanoplatelets buried in the Si wafer[18] by diffusion of Co atoms from the SiO_2/Si interface.

TEM

After having deposited Co-doped SiO_2 thin films on Si(001), Si(111) and Si(011) wafers, all samples subjected to the same thermal treatment were analyzed by TEM. Cross-sectional TEM specimens were prepared at different zone-axis by a combined process of mechanical polishing and Ar-ion milling. Figure 1 shows TEM images of the Si(001) substrate and the deposited SiO_2 thin film. In Figure 1a we can identify the presence of NP embedded in the SiO_2 thin film and also thin nanoplatelets buried in the Si(001) wafer. Figures 1b to 1d confirm this plate-like shape, where the TEM specimen was tilted by 0, 15 and 30 degrees, respectively. Figure 1d shows a nanoplatelet in a front view. Additional TEM images are displayed in Figure S2 in SI.
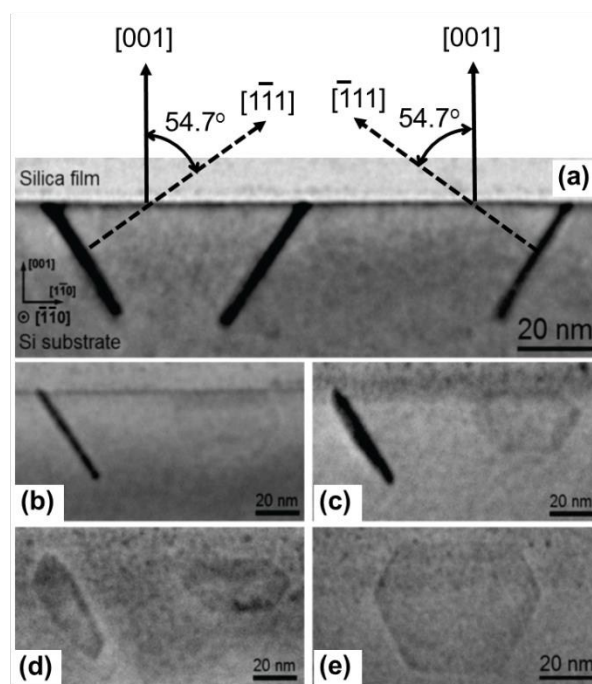

Figure 1. TEM images of SiO_2 thin film deposited on a Si(001) at [110] oriented zone axis (a) and tilted at increasing angles – (b) 0°, (c) 15° and (d) 30°. These images show different views of $CoSi_2$ nanoplatelets in which their hexagonal shape is clearly apparent. The main surfaces of the $CoSi_2$ nanoplatelets buried in Si(001) are all of them parallel to one of the planes of the Si{111} crystallographic form.

TEM images shown in Figure 1 exhibit the same overall features as those corresponding to a previous study of a similar sample, namely Co NP randomly dispersed in the SiO_2 thin film and $CoSi_2$ nanoplatelets regularly buried in the Si(001) wafer[18]. In the mentioned previous work it was also demonstrated that the $CoSi_2$ nanoplatelets exhibit a CaF_2 crystallographic structure and their lattices are coherently

related to the cubic lattice of the host Si matrix. We notice in Figure 1 that the angle between the main faces of all observed CoSi$_2$ nanoplatelets and the Si(001)/SiO$_2$ interface is $\alpha = 54.7^o$, this value being the angle between each plane of the Si{111} crystallographic form and the Si(001) plane. These observations confirm the previous results stating that the main faces of all CoSi$_2$ nanoplatelets buried in the Si(001) wafer are oriented parallel to crystallographic planes of the Si{111} form[18], exhibiting a four-fold rotation symmetry around the Si[001] crystallographic direction.
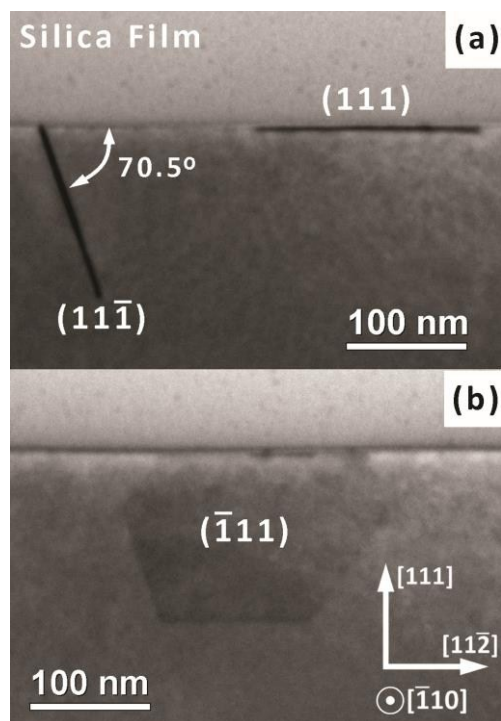

Figure 2: STEM bright field images corresponding to SiO$_2$ thin film with Co nanoparticles deposited on Si(111) wafer, observed along the [-110] zone axis. The angle between each nanoplatelet main face with the external face of the Si wafer is $\alpha = 70.5^o$, which is the expected angle between the [111] direction and one of the other three crystallographic directions normal to planes of the {111} crystallographic form. A nanoplatelet lies on the surface of the wafer, i. e. $\alpha = 0$.

TEM image corresponding to the second studied sample using this time a Si(111) substrate is shown in Figure 2. In these images, observed along a [-110] zone axis the presence of Co NP embedded in the SiO$_2$ thin film and CoSi$_2$ nanoplatelets buried in the Si(111) wafer with different orientations are also apparent. The angles between the main faces of the observed nanoplatelets and the Si/SiO$_2$ interface are close to $\alpha = 70.5^\circ$, as depicted on Figure 2a for a nanoplatelet grown at $\left(11\bar{1}\right)$ plane. Additionally, Figure 2a image also show CoSi$_2$ nanoplatelets lying on the external surface of the wafer, i.e. parallel to the crystallographic Si(111) plane. The analysis of several TEM images demonstrate that the normal to the main surfaces of the observed CoSi$_2$ nanoplatelets exhibit a 3-fold rotation symmetry around the Si[111] direction, as evidenced by the nanoplatelet at $\left(\bar{1}11\right)$ plane in Figure 2b. Similarly to what it was established for the CoSi$_2$ nanoplatelets buried in a Si(001) substrate, in the case of those in a Si(111) substrate, our results demonstrated that their main faces are also parallel to crystallographic planes of the Si{111} form. Additional images are shown on SI material, where this sample is observed along the $[11\bar{2}]$ zone axis. On this image one can observe a nanoplatelet in a front-view at the $\left(11\bar{1}\right)$ plane.

Finally, a third TEM analysis of samples corresponding to a Co-doped thin film deposited on a Si(011) wafer was performed (not shown here). In this third sample observed at the $[2\bar{1}1]$ zone axis, we have detected the presence of Co NP embedded in the SiO$_2$ thin film and CoSi$_2$ nanoplatelets buried in the Si(011) wafer with different orientations, some of them making an angle $\alpha = 35.3^o$ and others an angle $\alpha = 90^o$, with respect to the Si(011)/SiO$_2$ interface. The directions normal to the CoSi$_2$ nanoplatelets exhibit in this case a 2-fold rotation symmetry around the Si[011] axis. These angles, $\alpha_1 = 35.3^o$ and $\alpha_2 = 90^o$, are the expected angles between the different planes of the Si{111} crystallographic form and the plane Si(011). Again in this case our results of TEM analysis demonstrate that the main faces of all CoSi$_2$ nanoplatelets are parallel to crystallographic planes belonging to the Si{111} form.

All of these results indicates that irrespective of the type of Si crystal, namely Si(001), Si(111) and Si(011), the main faces of the buried CoSi$_2$ nanoplatelets are, in all cases, parallel to Si{111} crystallographic planes. Both symmetry and orientation of the buried CoSi$_2$ nanoplatelets could be easily identified by the use of stereographic projections of crystallographic planes of the cubic Si{111} form in each type of crystal. These aspects are summarized in SI (Figure S3).

GISAXS

In order to achieve a complementary characterization of the CoSi2 nanoplatelets buried in Si over a large surface area, we have performed GISAXS measurements on the same three samples as those previously studied by TEM. 2D GISAXS patterns corresponding to samples consisting of Co-doped SiO2 thin films deposited on Si(001), Si(011) and Si(111) substrates are shown in Figures 3(a), (b) and (c), respectively.
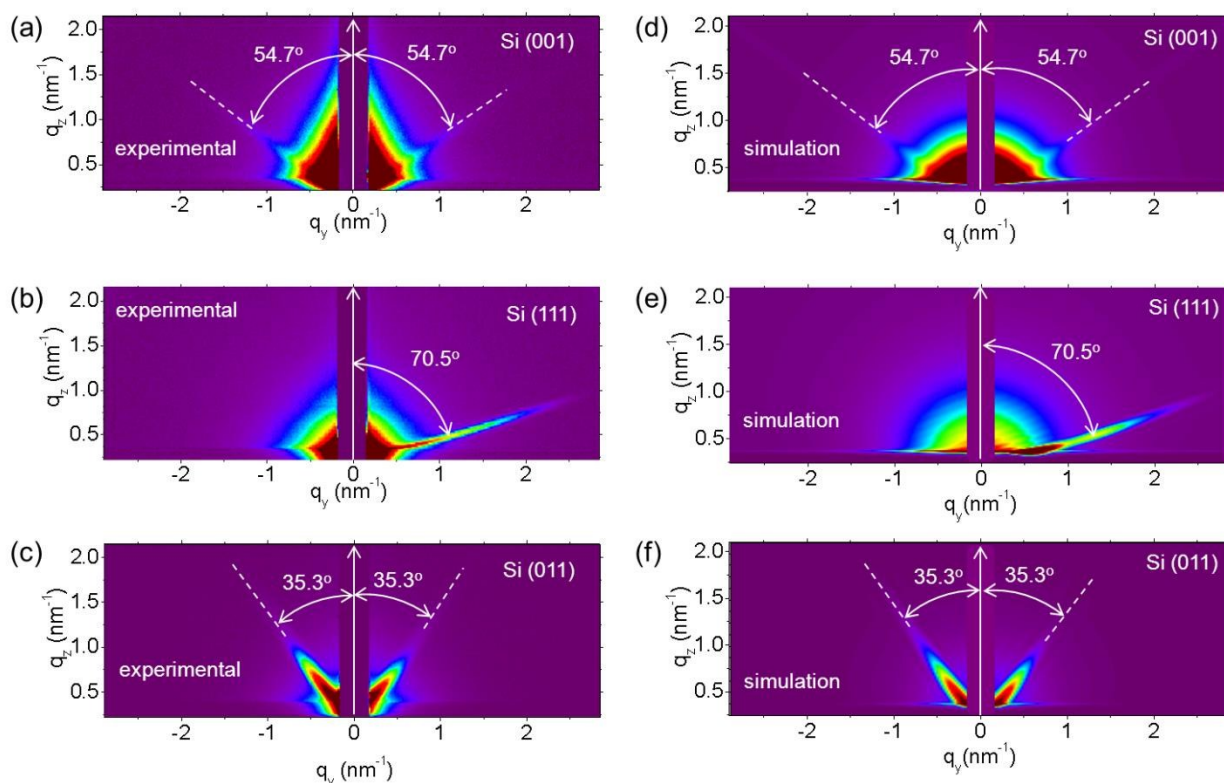
Figure 3: Experimental GISAXS 2D patterns corresponding to samples consisting of SiO_2 thin films deposited on (a) Si(001), (b) Si(111) and (c) Si(011) wafers. In addition to a diffuse scattering produced by the Co NP, narrow lobes with their maximum length along directions perpendicular to the Si{111} crystallographic planes are apparent in all patterns (see in text the description for each case). The right column - figures 3(d), (e) and (f) - are the calculated 2D GISAXS intensity patterns using the parameters determined from the best fitting procedure for experimental GISAXS intensity profiles corresponding to Si(001), Si(111) and Si(011) wafers, respectively.

In all these GISAXS patterns we have noticed that, in addition to an isotropic scattering produced by the Co NP embedded in the SiO2 thin films, narrow and elongated intensity lobes appear in one or two directions in reciprocal space. These lobes are a priori the expected contribution to GISAXS intensity from the anisotropic set of thin $CoSi_2$ nanoplatelets previously observed in TEM images. Notice that the scattering intensity produced by a thin platelet with a given orientation is expected to be concentrated, in the reciprocal space, within a narrow lobe with its maximum dimension perpendicular to the plane defined by the main nanoplatelet face.

By proper rotations of the sample around the z axis, we could visualize the lobes exhibiting in the detection plane their maximum length. In addition we have verified that the GISAXS patterns for the three studied samples, Si(001), Si(111) and Si(011), are repeated for rotation angles $\phi_{001}=90^o$, $\phi_{111}=120^o$ and $\phi_{011}=180^o$ around the z-axis, corresponding to 4-fold, 3-fold and 2-fold rotation symmetries, respectively. These findings imply that the general features of our GISAXS results fully

agree with the conclusions previously derived from TEM analysis. This additionally implies that the reported structure exists inside the whole region of the Si crystals illuminated by the X-ray beam, close to the external surface and over an area of at least 60 mm^2.

In Figure 3(a) the ϕ angle was adequately selected for obtaining an approximately symmetric pattern. The same pattern is in this case obtained after subsequent 90° for ϕ rotations. In Figure 3(b) only a narrow lobe is apparent at right. The same lobe appears at left after rotations with $\phi = 60^o$ or -60°. The non-symmetric pattern shown in Figure 3(c) was obtained by properly varying the ϕ angle to record the lobe at the left along its maximum length.

In Figure 3(a), (b) and (c) we have indicated the angles between the z-direction, corresponding to Si[001], Si[111] and Si[011], respectively, and the directions along the maximum diameter of the scattering intensity lobes. These angles are close to 54.7^o, 70.5^o and 35.3^o for the GISAXS patterns corresponding to Si(001), Si(111) and Si(011), respectively. These measured values are the crystallographic angles between the directions related to the cubic {111} crystallographic form - i.e. [111], [$\bar{1}$11], [1$\bar{1}$1], [11$\bar{1}$] - and the [001], [111] and [011] directions, respectively. Notice that the scattering intensity lobes expected for the (111) crystallographic plane in the Si(111) wafer and the (11$\bar{1}$) and (1$\bar{1}$1) planes in Si(011) wafer are not apparent in our GISAXS patterns due to the hiding effects of the vertical beam-

stopper and the sample shadow, respectively. These results quantitatively confirm our previous conclusion from TEM analysis stating that for the three differently oriented Si wafers studied here, all hexagonal $CoSi_2$ nanoplatelets are exclusively oriented with their main surface parallel to planes of the Si{111} crystallographic form.

Based on TEM results and preliminary GISAXS analyses, in order to quantitatively determine size and size distribution of Co NP and orientations, thicknesses and lateral dimensions of the $CoSi_2$ nanoplatelets, we have proposed a simple model for the nanostructure developed in the studied materials as being composed of a isotropic and dilute set of spherical Co NP embedded in a homogeneous SiO_2 thin film and an also dilute and anisotropic set of thin $CoSi_2$ nanoplatelets with hexagonal lateral shape, buried in a homogeneous Si single crystal matrix and parallel to all planes of the Si{111} crystallographic form. A detailed description of the proposed analysis can be found in SI.

lateral size and a thickness distribution given by a Gaussian function, and (ii) the spherical Co NP exhibit a radius distribution described by a lognormal function.

A good agreement between the experimental GISAXS data and the best fitted curves was obtained for all samples and all exit α_f angles, over a wide q range except at very low q values of the in-plane scattering vector (near the beam-stopper shadow) where the measured scattering intensity is higher than that predicted by our model. The 2D GISAXS intensity calculated using the best fitting parameters for the three investigated crystallographic orientations of the surface of the single crystalline Si samples, Si(001), Si(111) and Si(011), are shown in Figures 3(d), (e) and (f), respectively. Except over the very small q_y region of the GISAXS intensity curves corresponding to the Si(001) sample, the calculated (modelled) GISAXS intensity functions exhibit a good agreement with the measured patterns. The observed discrepancy occurs over the low q region for which a significant contribution from the totally reflected beam is expected.
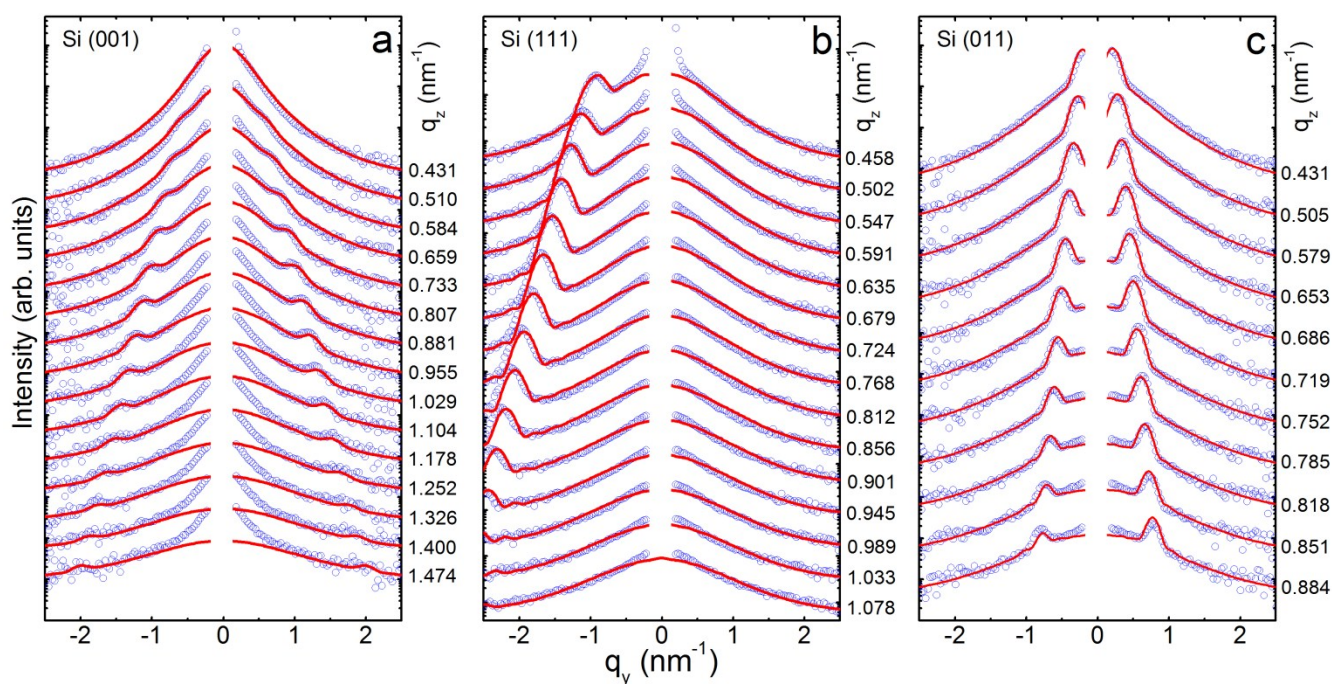

Figure 4: Experimental GISAXS profiles $I \times q_y$ (symbols) and modelled scattering intensity curves (solid lines) associated to several horizontal cuts at the detection plane for the indicated q_z values. Figures 4(a), (b) and (c) display the GISAXS results corresponding to Si(001), Si(111) and Si(011) wafers, respectively.

By applying the best fit procedure of the SAXS intensity curves theoretically expected for the proposed model to the experimental scattering intensity data, we were able to determine the size distributions of Co NP and $CoSi_2$ nanoplatelets corresponding to the three studied samples. Figure 4(a), (b) and (c), exhibit the GISAXS intensity curves, I $\times q_y$, recorded for different values of the exit angle α_f (symbols). In the same figure, the solid lines are the modelled GISAXS curves corresponding to the best fitting obtained. We have assumed for this modelling that: (i) the $CoSi_2$ nanoplatelets have a regular hexagonal shape with the same

The structural parameters associated to the modeled GISAXS curves that best fitted our experimental results, related to the three different orientations of the Si substrate, are summarized in Table 1. The large difference between experimental and modelled scattering GISAXS intensity curves, at very small q, in the case in which the film is deposited on a Si wafer (100) see Figure 4(a) can be attributed to two possible reasons. One of them is the relatively low contribution to the scattering intensity from spherical Co particles as compared to the diffuse intensity of the reflected beam. Another additional explanation is due to the presence of a rather large population of large Co particles thus leading to an additional contribution to GISAXS intensity at very small q values.

The values of the lateral size and thickness of the hexagonal nanoplatelets corresponding to the sample deposited on the

Si(001) wafer are close to those obtained in our previous study for the same Si orientation[18]. The small relative dispersion in the nanoplatelet thickness $\sigma_t/\langle t \rangle = 0.14$ obtained for Si(001) wafer, confirms the rather small thickness dispersion in this parameter as previously reported.

Table 1: Structural parameters determined from the analysis of experimental GISAXS results corresponding to thin films deposited on three different Si substrates, namely Si(001), Si(111) and Si(011).

Si external surface	D(nm) [a]	$\langle t \rangle$ (nm) [b]	$\sigma_t / \langle t \rangle$ [c]	$\langle R \rangle$((nm) [d]	$\sigma_R /\langle R \rangle$ [f]
001)	28.0	2.8	0.14	1.5	0.7
(111)	40.0	5.7	0.18	1.0	0.5
(011)	28.0	5.0	0.24	0.6	0.6

Parameters related to the CoSi$_2$ nanoplatelets buried in the Si single crystals are [a]D lateral size, [b]$\langle t \rangle$ Average thickness and [c]$\sigma_t/\langle t \rangle$ dispersion/thickness ratio. The parameters associated to the Co nanoparticles embedded in the SiO$_2$ thin films are [d]$\langle R \rangle$ average radius and [f]$\sigma_R/\langle R \rangle$ relative radius dispersion.

On the other hand, in spite of the identical conditions for deposition on the three substrates, the results reported in table 1 indicate that the lateral size and thickness of nano-hexagons depend on the crystallographic orientation of the external surface of the Si wafer. A particularly remarkably high difference is observed for nanoplatelets deposited on the Si(111) wafer, the lateral average sizes and the thickness of these nanoplatelets being much larger than those corresponding to platelets buried in Si the (001) wafer. This indicates that the diffusion of Co atoms and subsequent formation of buried CoSi$_2$ platelets are greatly enhanced in Si(111) substrates.

The average radius of the spherical Co NP embedded in the SiO2 thin films determined from the best fit of the modeled GISAXS function to our experimental data are 1.5 nm, 1.0 nm and 0.6 nm for Si (001), Si (111) and Si (011) substrates, respectively. On the other hand the relative dispersion of NP sizes - i.e. the ratio between the standard deviation and the average radius - ranges from 0.5 up to 0.7 for the different studied samples.

Conclusions

The presented TEM study of nanostructured composites consisting of either Si(001), Si(011) and Si(111) wafers in which Co-doped SiO$_2$ thin films were deposited under the same conditions and submitted to equivalent thermal treatments, demonstrated the spontaneous formation in all cases of: (i) spherical Co NP embedded in the SiO$_2$ thin films and (ii) CoSi$_2$ nanoplatelets buried into the Si substrates. All observed CoSi$_2$ nanoplatelets exhibit a hexagonal lateral shape with one of their sides in contact with the Si/SiO$_2$ interface. TEM images also demonstrated that regardless of the Si/SiO$_2$ interface orientation, the large faces of the buried CoSi$_2$ nanoplatelets are in all cases parallel to crystallographic planes of the Si{111}form.

On the other hand, our GISAXS results fully agree with the finding derived from TEM images regarding the formation of Co NP embedded in the SiO$_2$ thin films and the general features of the CoSi$_2$ nanoplatelets buried in either Si(001), Si(011) and Si(111) substrates.

We can understand that the diffusion of Co atoms only occurs along {111} planes in the three studied Si wafers because the observed CoSi$_2${111}/Si{111} interfaces exhibit a surface energy lower than those corresponding to the interfaces with other Si crystallographic planes[19]. The formation of CoSi$_2$ island epitaxially grown on the surface of Si single crystals has been previously reported[20–23], but the formation of such islands forming endotaxially grown nanoplatelets by diffusion of Co atoms into Si along Si{111} planes, regardless the orientation of the silicon crystal, was - to our knowledge - not previously reported. Moreover, Mahato et al.[23] observed the spontaneous change of shape of epitaxial CoSi$_2$ islands on Si(100) while treated at 600 °C in UHV, this effect leading to the formation of CoSi$_2$ endotaxial nanowires. The formation of nanoplatelets observed in our case is reached after a heat treatment at higher temperature, at least 650 °C. At these temperatures, the observed CoSi$_2$ nanoplatelets are probably developed by the growth of precursor endotaxial CoSi$_2$ nanowires[23] along Si{111} crystallographic planes, this structural transformation being driven by a decrease in overall elastic stresses in bulk Si. The quantitative analysis of GISAXS measurements indicates that the spherical Co NP embedded in the SiO$_2$ thin films have average radii ranging from 0.6 nm for thin films deposited on Si(011) up to 1.5 nm for those deposited on Si(001).

Additionally, our GISAXS results demonstrated that the sizes of the CoSi$_2$ nano-hexagons buried in Si wafers depend on the crystallographic orientation of the Si/SiO$_2$ interface, the lateral size of the nano-hexagons in Si(111) being remarkably (~50%) higher than those formed in Si(111) and Si(011). The thickness of the CoSi$_2$ nanoplatelets also varies for different Si substrate orientations from 2.8 nm for Si(001) up to 5.7 nm for Si(111). The sizes of the CoSi2 hexagonal nanoplatelets are expected to depend on the density of Co in the SiO2 thin film, which were not well controlled during our synthesis. New experiments controlling the amount of deposited Co by spin-coating deposition is presently under way.

Notes and references
[a] Departamento de Física, Universidade Federal do Paraná, Caixa Postal 19091, Curitiba, Paraná 81531-990, Brazil.

[b] Departamento de Química, Universidade Federal de Minas Gerais, 31270-901, Belo Horizonte, MG, Brazil.

[c] Instituto de Investigaciones Fisicoquímicas Teóricas y Aplicadas (INIFTA, CONICET, Departamento de Química, Facultad de Ciencias Exactas, Universidad Nacional de La Plata), CC/16 suc. 4, 1900 La Plata, Argentina.

[d] School of Chemical, Biological & Materials Engineering, University of Oklahoma, Norman, OK 73019, USA.

[e] Brazilian Nanotecnology National Laboratory (LNNano), Caixa Postal 6192 - CEP 13083-970, Campinas, São Paulo, 13083-100, Brazil.

[f] Institute of Physics, University of Sao Paulo, CP 66318, CEP 05315-970, São Paulo, Brazil.

1. R. C. Chau, B. Doyle, S. Datta, K. Jack and K. Zhang, *Nat. Mater.*, 2007, **6**, 810 – 812.
2. Z. Nie, A. Petukhova and E. Kumacheva, *Nat. Nanotechnol.*, 2010, **5**, 15–25.
3. H. S. Nalwa, *Handbook of Nanostructured Materials and Nanotechnology, Five-Volume Set*, .
4. H. Cölfen and S. Mann, *Angew. Chem. Int. Ed.*, 2003, **42**, 2350–2365.
5. Y. Lei, W. Cai and G. Wilde, *Prog. Mater. Sci.*, 2007, **52**, 465–539.
6. J. P. Gambino and E. G. Colgan, *Mater. Chem. Phys.*, 1998, **52**, 99–146.
7. J. A. Kittl, A. Lauwers, O. Chamirian, M. Van Dal, A. Akheyar, M. De Potter, R. Lindsay and K. Maex, *Microelectron. Eng.*, 2003, **70**, 158–165.
8. C. Lavoie, F. M. d' Heurle, C. Detavernier and C. Cabral Jr., *Microelectron. Eng.*, 2003, **70**, 144–157.
9. K. Kawamura, S. Inagaki, T. Saiki, R. Nakamura, Y. Kataoka and M. Kase, *Jpn. J. Appl. Phys.*, 2007, **46**, 7268.
10. L. J. Chen, *Silicide Technology for Integrated Circuits (Processing)*, IET, 2004.
11. L. J. Chen, *J. Oper. Manag.*, 2005, **57**, 24–31.
12. B. J. Sealy, B. L. Tan, R. M. Gwilliam, K. J. Reeson and C. Jeynes, *Electron. Lett.*, 1989, **25**, 1532–1533.
13. J. V. Barth, G. Costantini and K. Kern, *Nature*, 2005, **437**, 671–679.
14. D. Gentili, F. Valle, C. Albonetti, F. Liscio and M. Cavallini, *Acc. Chem. Res.*, 2014.
15. Y.-C. Chou, W.-W. Wu, L.-J. Chen and K.-N. Tu, *Nano Lett.*, 2009, **9**, 2337–2342.
16. H. Wang, Z. Zhang, L. M. Wong, S. Wang, Z. Wei, G. P. Li, G. Xing, D. Guo, D. Wang and T. Wu, *ACS Nano*, 2010, **4**, 2901–2909.
17. B. M. Boyerinas, A. L. Roytburd and H. A. Bruck, *Nano Lett.*, 2014, **14**, 1818–1822.
18. G. Kellermann, L. A. Montoro, L. J. Giovanetti, P. C. dos Santos Claro, L. Zhang, A. J. Ramirez, F. G. Requejo and A. F. Craievich, *Appl. Phys. Lett.*, 2012, **100**, 063116.
19. S. M. Yalisove, R. T. Tung and D. Loretto, *J. Vac. Sci. Technol. A*, 1989, **7**, 1472–1474.
20. M. Gomoyunova, I. Pronin, D. Valdaitsev and N. Faradzhev, *Phys. Solid State*, 2001, **43**, 569–573.
21. U. Zimmermann, J.-P. Schlomka, M. Tolan, J. Stettner, W. Press, M. Hacke and S. Mantl, *J. Appl. Phys.*, 1998, **83**, 5823–5830.
22. I. D. Kaendler, O. H. Seeck, J.-P. Schlomka, M. Tolan, W. Press, J. Stettner, L. Kappius, C. Dieker and S. Mantl, *J. Appl. Phys.*, 2000, **87**, 133–139.
23. J. C. Mahato, D. Das, R. R. Juluri, R. Batabyal, A. Roy, P. V. Satyam and B. N. Dev, *Appl. Phys. Lett.*, 2012, **100**, 263117.